20th European Symposium on Computer Aided Process Engineering – ESCAPE20
S. Pierucci and G. Buzzi Ferraris (Editors)

Particle Transfer and Deposition Using an Integrated CFD Model of the Respiratory System

Aleck H. Alexopoulos[a], Paraskevi Karakosta[a], Costas Kiparissides*[a]

[a]*Department of Chemical Engineering and Chemical Process Engineering Research, Aristotle University of Thessaloniki, P.O. Box 472, Thessaloniki, Greece,* cypress@cperi.certh.gr

Abstract

The present work describes an integrated CFD model of the respiratory system from the nasal cavity down to the bronchioli. The model is comprised of nine sequential computational blocks corresponding to the nasal cavity, the pharyngo-trachea, and a series of branches in the pulmonary system. Steady-state turbulent flow is employed to describe the inspiration flow and deposition of particles of different sizes. Local deposition efficiency is found to increase with particle size and flow rate. The deposition profiles are in accordance to experimental and computational results available in the literature. The proposed integrated respiratory model describes the flow, penetration, and deposition of particles in the respiratory system accounting for the influence of the nasal cavity and the pulmonary branches.

Keywords: respiratory, pulmonary, CFD, particles, deposition

1. Introduction

The transfer and deposition of particles in the respiratory system is of major interest for the development of targeted drug delivery formulations but also due to the increasing concerns over the potential toxicity of natural and engineered particles. Experimental and theoretical work have focused on different regions of the respiratory system, e.g., oropharyngeal, nasal, pulmonary, and alveolar, where many aspects of particle penetration are fairly well understood. However, several issues remain to be elucidated including the deposition of non-spherical particles and fibers, particle dispersion and aggregation, changes in particle size and shape and finally the fate of deposited particles. To further improve our understanding on particle penetration and deposition an integrated CFD model of the entire respiratory system has been developed and the detailed penetration and deposition of particles has been investigated.

In this work the respiratory system is assumed to consist of ten sequential computational blocks. The first block corresponds to the inflow cavity, e.g., the nasal or the oral cavity. The second block connects the inflow cavity to the lower trachea just above the first pulmonary bifurcation. The following seven blocks correspond to branching structures of the pulmonary system. The final computational block corresponds to the alveoli sacs and individual alveoli where gas exchange occurs. Flow and deposition of particles in the respiratory system is determined by performing CFD simulations in each computational block. The outflow conditions of a specific computational block are used as inflow conditions of the subsequent computational block. This paper deals with the simulation of steady-state nasal inspiration and particle deposition in the first nine blocks of the respiratory model.

2. CFD Simulations of the Respiratory System

The nasal cavity consists of two nasal air paths converging posteriorly to a single pathway, the nasopharynx, which is then directed downwards to the pharynx and the trachea. The two nasal air paths are highly curved and convoluted in shape providing a total surface area of about 150 cm^2. The nasal walls are covered by a mucous layer which moves to the posterior clearing deposited particles. The flow and deposition of particles in the nasal cavity has recently been investigated by several groups (Liu et al., 2007; Shi et al., 2008; Wen et al., 2008)**.**

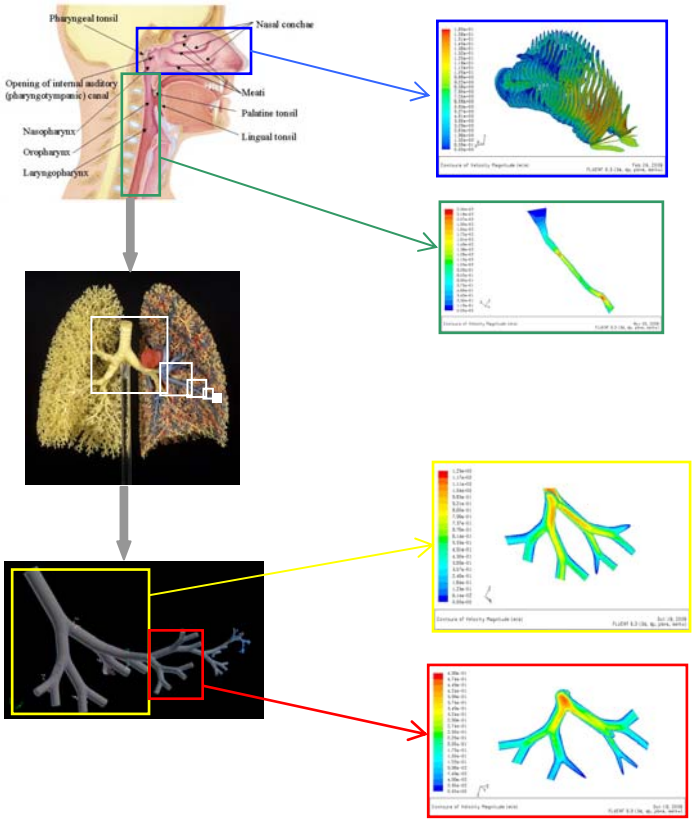

Figure 1. Block Computational Structure of the Respiratory System

The pharyngotracheal route can be studied not only to determine particle depositions but also to determine the function of the larynx. In terms of airflow it can be simplified to a curved conduit of changing cross-sectional area and shape. There are two main constrictions: one at the top of the oral cavity and the second near the larynx (Fig. 1). Most of the deposition occurs in these two regions.

The pulmonary system consists of a multitude of nonsymmetrical branches of progressively smaller diameter. There are a total of 23-24 branch generations leading to about 10^8 simple branches in the entire pulmonary system (Finlay, 2004). This limits the number of branch generations that can be completely simulated to around 5-6 (Longest and Vinchurkar, 2007; van Ertbruggen et al., 2005; Zhang et al., 2002). However, if a single pathline down to the alveolar sacs is considered, a successive simulation approach can be followed (Nowak et al., 2003).

In the present work, a model of the pulmonary tract is developed based on a sequence of seven consecutive "blocks" from the bronchi down to the alveolar sacs. Each block consists of four generations of symmetrical branches with one side rotated 90 degrees relative to the other. The inlet flow and particle motion conditions of each block are obtained from the outlet conditions of the previous block and the inlet conditions of the first block of the pulmonary system are obtained from the outlet conditions of the pharygotracheal block. Particle depositions in the pulmonary tract favor the larger particles with only the smallest of particles reaching the lower respiratory tract and alveolar sacs at significant concentrations.

3. Results and Discussion

Results are presented for the velocity magnitude and the local particle deposition efficiency in the nasal cavity, the pharyngotrachea, and the initial blocks of the pulmonary system. Particle deposition is determined by a Eulerian/Lagrangian tracking scheme based on the steady-state solutions for flow. Both uniform and Rosin-Rammler size distributions are employed.

3.1. Results for the Nasal Cavity

In this work, the nasal cavity geometry is reconstructed based on a series of medical images and is similar to the geometry described in Shi et al. (2008). A number of different computational grids consisting of tetrahedral cells were generated varying from about 3 10^5 to 2 10^6 in number with a distortion of less than 0.8. Because of the transitional nature of the flow in the nasal cavity the transitional k-ω model was employed as it is a good compromise between laminar and fully-developed turbulent flow. Inflow conditions to the nasal cavity were taken to be either constant or parabolic.

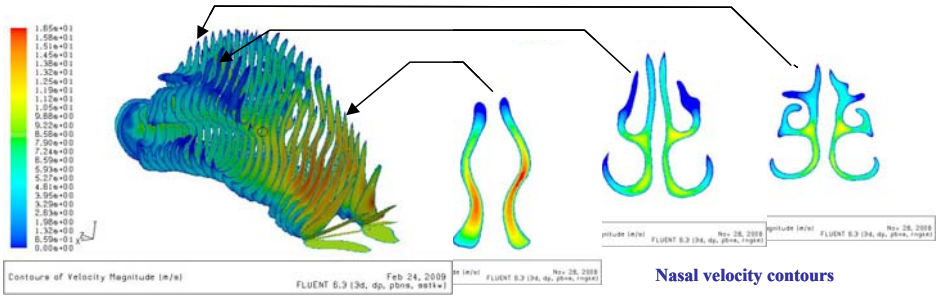

Figure 2. Velocity magnitude in the nasal cavity. Coronal sections. Inlet velocity V_{in}=2m/s.

The velocity magnitude at different coronal slices is obtained for different inlet velocites. As can be seen in Fig. 2 the incoming air-flow accelerates up to the nasal valve after which it decelerates and is directed towards the intersection of the nasal meatuses where the cross-sectional area is largest and the resistance to flow the lowest. This flow pattern permits adequate mixing up to the sensitive olfactory region, situated in the upper region of the nasal cavity, while at the same time leads to a large capture rate of large (i.e., >5μm) particles.

For inertia-dominated cases, particle deposition efficiency is typically described in terms of the impaction parameter, QD^2, where Q is the volumetric flow rate and D the particle diameter. Comprehensive information on the axial and size distribution of deposited particles is obtained (Fig. 3). It is found that larger particles are mostly

deposited in the anterior region of the nasal cavity while smaller particles were deposited less yet more evenly throughout the entire nasal cavity.

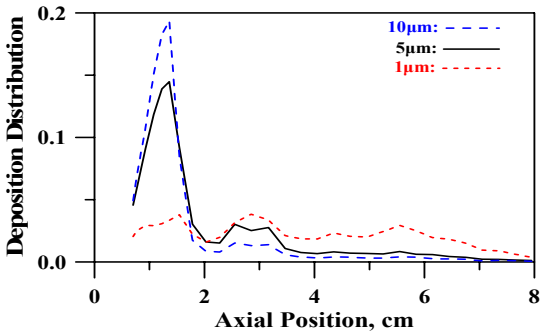

Figure 3. Particle Deposition Profiles in the Nasal Cavity. Inlet velocity V_{in}=2m/s.

3.2. Results for the PharyngoTrachea

The computational geometry was obtains by extending the nasopharyngeal region of the posterior nasal cavity downwards towards the pharynx and trachea. The geometric description of Heenan et al. (2003) was employed without the oral cavity and with the laryngeal region smoothed to obtain a computational grid consisting of 88,000 tetrahedral cells.

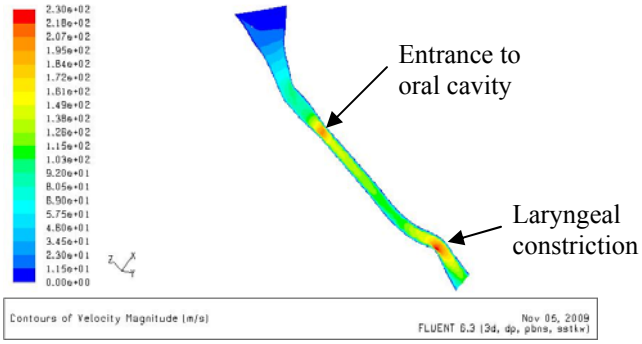

Figure 4. Velocity Magnitude, V_{in}=5m/s.

As can be seen in Fig. 4 the velocity of airflow accelerates in the converging nasopharyngeal region. Peak velocities are observed at pharyngotracheal positions corresponding to narrow cross-sectional positions observed just above the oral cavity and in the laryngeal region. Particle depositions increased with particle size and flow rate and occurred mostly in the regions of constricted and fast flow.

3.3. Results for the Pulmonary System

In the present work, a model of the pulmonary tract is developed based on 7 consecutive "blocks" of the pulmonary system. Each block consists of 4 generations of symmetrical branches with one side rotated 90 degrees relative to the other and is discretized into 260,000 tetrahedral cells. To examine the sensitivity of block selection on the final solution different computational geometries and grids were constructed by altering the sequence of blocks.

In Fig. 5 the velocity magnitudes are shown for blocks one and four of two different geometries (i.e., block sequence). It is clear that the velocity magnitudes are significantly different between block one and block four for both geometries. Moreover, the differences in the calculated velocity magnitudes between two different geometries are significant for the first block. On the other hand, the flows are nearly identical in the fourth block for both geometries. Therefore, block selection during the assembly of the pulmonary geometry is important only in the first two blocks of the pulmonary system.

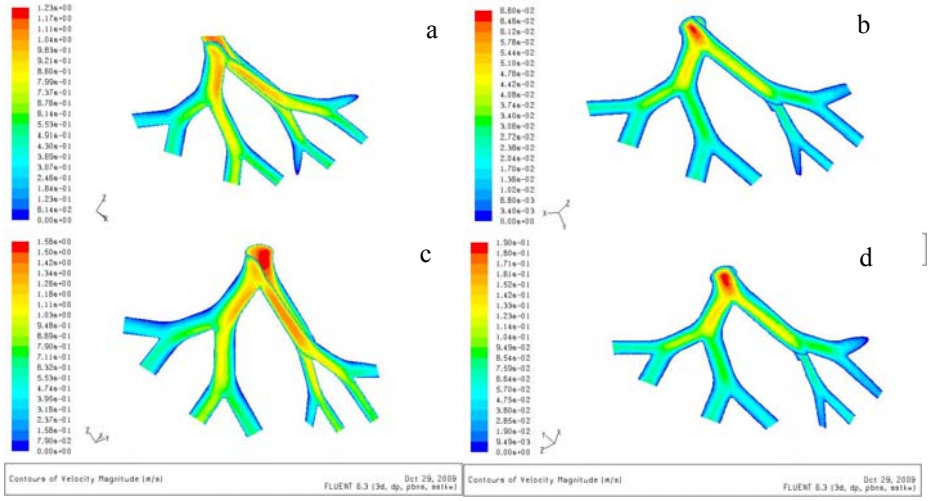

Figure 5. Velocity magnitudes for different blocks and geometries, V_{in}=2.7m/s. First block (a) and (c). Fourth block (b) and (d). Geometry one (a) and (b). Geometry two (c) and (d).

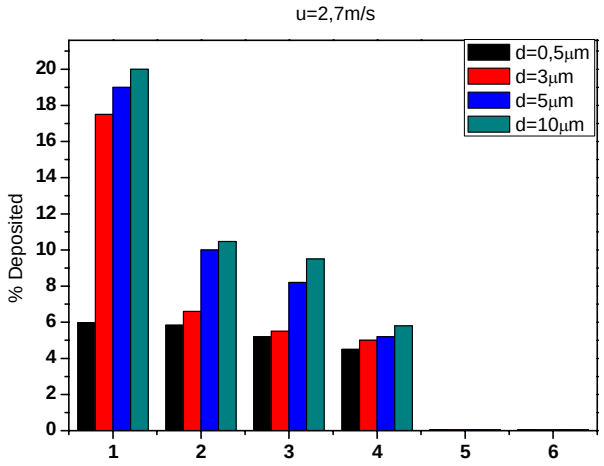

Figure 6. Local Deposition Efficiency in the Pulmonary System V_{in}=2.7m/s.

The calculated local deposition efficiencies for each computational block are displayed in Fig. 6. As can be seen, the local deposition efficiency decreases with each successive block due to a decrease in the value of the flow rate. On the other hand, for each block the local deposition efficiency increases with particle size from 500nm to 10μm. The results for blocks five and six are not shown due to the inadequate resolution of particle

deposition given that only a small number of particles reached these blocks. These results for local particle deposition are in qualitative agreement to the results reported in the literature, e.g., Nowak et al. (2003), and are consistent to an inertia dominated deposition mechanism which is expected for micron-sized particles.

4. Conclusions

In conclusion the sequential block approach, despite its many simplifications, can describe flow and deposition profiles in the respiratory system. The choice of pulmonary blocks is shown to be important only in the first two blocks of the pulmonary system. Therefore, realistic physiological representations should only be performed for the upper respiratory tract. Deposition of large (i.e., >1μm) particles are inertially dominated and scale with QD^2. The deposition of smaller particles (i.e., <1μm) is more complicated as diffusional forces becomes important. The computed particle deposition profiles in terms of local deposition efficiency appear to be in qualitative agreement with experimental and computational data.

Future work will involve the description of ellipsoidal particles and investigate the effect of surface charge. The alveolar sacs and individual alveoli will also be included to the integrated model of the respiratory system and the simulations will be extended to a full breathing cycle (i.e., inhalation and exhalation).

References

W.H. Finlay, 2004, Lung Deposition Simulation, in A.J. Hickey (ed.) Pharmaceutical Inhalation Aerosol Technology, Marcel Dekker, NY 2004.

A.F. Heenan, E. Matida, A. Pollard, and W.H. Finlay, 2003, Experimental measurements and computational modeling of the flow in an idealized human oropharynx. Experiments in Fluids, 35, 70-84.

Y. Liu, E.A. Matida, J. Gu and M.R. Johnson, 2007, Numerical simulation of aerosol deposition in a 3-D human nasal cavity using RANS, RANS/EIM, and LES, Aerosol Sci., 38, 683-700.

P. Longest and S.Vinchurkar, 2007, Validating CFD predictions of respiratory aerosol deposition: Effects of upstream transition and turbulence, J. of Biomechanics, 40(20), 305-316.

T.B. Martonen, Z. Zhang, G. Yue, and C.J. Musante 2002. 3-D particle transport within the human upper respiratory tract. Aerosol Science, 33, 1095-1110.

N. Nowak, P.P. Kakade and A.V. Annapragada, 2003, Computational Fluid Dynamics Simulation of Airflow and Aerosol Deposition in Human Lungs", Annals of Biomed. Engineering, 31, 374-390.

H.W. Shi, C. Kleinstreuer and Z. Zhang, 2008, Dilute suspension flow with nanoparticle deposition in a representative nasal airway model, Physics of Fluids 20, 013301.

C. van Ertbruggen, C. Hirsch and M. Paiva, 2005, Anatomically based three-dimensional model of airways to simulate flow and particle transport using computational fluid dynamics, J. Appl. Physiol., 98, 970-980.

J. Wen, K. Inthavong, J. Tu and S. Wang, 2008, Numerical simulations for detailed airflow dynamics in a human nasal cavity, Respiratory Physiology & Neurobiology.

G. Yu, Z. Zhang and R. Lessmann, 1998, Fluid Flow and Particle Diffusion in the Human Upper Respiratory System, Aerosol Science and Technology, 28(2),146-158.

Z. Zhang, C. Kleinstreuer and C.S. Kim, 2009, Comparison of analytical and CFD models with regard to micron particle deposition in a human 16-generation tracheobronchial airway model, Aerosol Science, 40, 16-28.